Collisions of unequal mass black holes and the point particle limit

Ulrich Sperhake,[1,2,3,*] Vitor Cardoso,[2,4] Christian D. Ott,[3] Erik Schnetter,[5,6,7,8] and Helvi Witek[2]

[1]*Institut de Ciències de l'Espai (CSIC-IEEC), Facultat de Ciències, Campus UAB, E-08193 Bellaterra, Spain*
[2]*CENTRA, Departamento de Física, Instituto Superior Técnico, Universidade Técnica de Lisboa - UTL, Av. Rovisco Pais 1, 1049 Lisboa, Portugal*
[3]*California Institute of Technology, Pasadena, California 91125, USA*
[4]*Department of Physics and Astronomy, The University of Mississippi, University, Mississippi 38677, USA*
[5]*Perimeter Institute for Theoretical Physics, 31 Caroline St. N., Waterloo ON N2L 2Y5, Canada*
[6]*Department of Physics, University of Guelph, 50 Stone Road East, Guelph, ON N1G 2W1, Canada*
[7]*Center for Computation & Technology, 216 Johnston Hall, Louisiana State University, Baton Rouge, Louisiana 70803, USA*
[8]*Department of Physics & Astronomy, 201 Nicholson Hall, Louisiana State University, Baton Rouge, Louisiana 70803, USA*

(Received 31 May 2011; published 18 October 2011)

Numerical relativity has seen incredible progress in the last years, and is being applied with success to a variety of physical phenomena, from gravitational wave research and relativistic astrophysics to cosmology and high-energy physics. Here we probe the limits of current numerical setups, by studying collisions of unequal mass, nonrotating black holes of mass ratios up to 1:100 and making contact with a classical calculation in general relativity: the infall of a pointlike particle into a massive black hole. Our results agree well with the predictions coming from linearized calculations of the infall of pointlike particles into nonrotating black holes. In particular, in the limit that one hole is much smaller than the other, and the infall starts from an infinite initial separation, we recover the point-particle limit. Thus, numerical relativity is able to bridge the gap between fully nonlinear dynamics and linearized approximations, which may have important applications. Finally, we also comment on the ''spurious'' radiation content in the initial data and the linearized predictions.

DOI: 10.1103/PhysRevD.84.084038 PACS numbers: 04.25.D−, 04.25.dg, 04.25.Nx, 04.30.−w

I. INTRODUCTION

Black holes (BH) play a key role in a variety of processes in astrophysics, gravitational wave physics and high-energy physics. Following the 2005 breakthroughs [1–3], numerical relativity has been an essential tool in the modeling of black-hole binaries in the strong-field regime. At the same time it has become clear that detailed studies of black-hole systems often involve a close interplay between fully nonlinear numerical simulations and (semi)-analytic approximation techniques of various types. For example, the generation of gravitational wave (GW) template banks for use in the analysis of observational data from laser interferometric GW detectors LIGO, VIRGO, GEO600, LCGT or LISA requires the combination of numerical relativity with post-Newtonian or other techniques; see Refs. [4–11] and references therein. Post-Newtonian studies have also played an important role in the guidance of the numerical investigation of the black-hole recoil, most notably in the discovery of the so-called *superkicks* and their possible suppression due to spin alignment [12–16]. In the context of high-energy collisions of black holes, linearization tools such as the zero-frequency limit or point-particle calculations provide valuable insight into the scattering threshold and GW emission of black-hole collisions in four and higher-dimensional spacetimes [17]. A particular class of black-hole binaries of high relevance for the spaceborne LISA (or a similar future spaceborne) observatory, the so-called extreme-mass-ratio inspirals, represent a particularly difficult challenge to numerical relativity and their modeling relies heavily on perturbative methods and self-force calculations; see Refs. [18–23] and references therein.

With the above as motivation, it is vital to obtain a detailed understanding of the range of validity of the various types of approximation methods. At the same time, these methods provide valuable tools to calibrate the accuracy of numerically generated solutions to the Einstein equations. The purpose of this paper is to provide such a study for the case of a classical calculation in general relativity, the head-on infall of a point-particle (PP) into a black hole [24].

In recent years, numerical relativity has started probing the intermediate mass-ratio regime by evolving the final orbits of (approximately) quasicircular inspirals of black-hole binaries with mass ratio $q \equiv m_2/m_1 = 1/10$ [25,26]; by comparing numerical results with perturbative calculations employing the fully numerical black-hole trajectories for mass ratios up to $q = 1/20$ [27] and most recently, mass ratios up to $q = 1/100$ [28,29] In this work, we restrict our attention to the head-on case of the collision of black holes, for two reasons: (i) the lower computational cost due to the higher degree of spacetime symmetry and the absence of the lengthy inspiral phase and (ii) the availability of high-precision results in the PP limit.

*sperhake@ieec.uab.es

In our study we will make extensive use of the calculation by Davis *et al.* [24] who model in the PP limit the collision of a small object of mass m with a black hole of mass $M \gg m$. In the original calculation the particle was falling from rest at infinity, and the total radiated energy was found to be

$$E_{\rm PP}^{\rm rad} = 0.0104 \frac{m^2}{M}. \quad (1)$$

This setting has been generalized to arbitrary initial distance and boost, in which case initial data and consequent spurious radiation play a role [17,30–33].

Fully numerical results for black-hole head-on collisions obtained in the equal and comparable mass regime have been compared with PP predictions and results obtained in the close-limit approximation [34] by Anninos and collaborators [35,36]. These studies demonstrated agreement for the radiated energy and linear momentum bearing in mind the accuracies achievable at the time. The wave forms presented therein, however, exhibit a significant signal starting at $t - R_{\rm ex} = 0$; see, for example, Fig. 1 in [36]. This contribution most likely arises from spurious radiation inherent in the initial data due to the small initial separation and its impact on the quantitative conclusions is not entirely clear.

Also, we are not aware of any comparisons between PP calculations and fully numerical results for mass ratios in a truly perturbative regime (as mentioned above, $q = 1/100$ simulations of inspiralling binaries have been reported in Refs. [28,29] and used for the construction of gravitational wave forms from the numerically generated BH trajectories.) By simulating black-hole binaries up to a mass ratio of $q = 1/100$ we fill this gap and identify those aspects of the PP predictions which describe black-hole dynamics well in general and which only hold in the extreme mass-ratio limit. From a different point of view, the agreement with the PP calculations represents an important validation of the fully numerical calculations in the regime of high-mass ratios. In this context we emphasize that we are able to accurately extract from binary black-hole simulations radiated GW energies of the order of $10^{-6}M$ and linear momenta corresponding to recoil velocities of a few dozens of m/s, similar to the average speed of a normal car. We note, however, that even smaller amounts of energy have been extracted from general relativistic simulations of stellar core collapse; see e.g. [37].

This paper is organized as follows. We summarize our numerical framework in Sec. II, estimate numerical uncertainties in Sec. III, describe our results in Sec. IV and conclude in Sec. V.

II. NUMERICAL SETUP AND ANALYSIS TOOLS

The numerical simulations of unequal mass black-hole collisions starting from rest have been performed with the LEAN code, originally introduced in Refs. [38,39]. The LEAN code is based on the CACTUS computational toolkit [40,41] and uses the CARPET mesh refinement package [42,43], the apparent horizon finder AHFINDERDIRECT [44,45] and the TWOPUNCTURE initial data solver [46]. The $3 + 1$ Einstein's equations are evolved using the Baumgarte-Shapiro-Shibata-Nakamura [47,48] formulation, together with the moving puncture approach [2,3]. The gauge conditions are determined by the so-called puncture gauge, i.e., the "$1 + \log$" slicing and Γ driver shift condition [49]. The systems are set up using Brill-Lindquist initial data. We have evolved BH binaries with mass ratios $q \equiv m_2/m_1 = 1, 1/2, 1/3, 1/4, 1/10$ and $1/100$, where m_i is the bare mass parameter of the i-th BH.

We use the Newman-Penrose scalar Ψ_4 to measure gravitational radiation at extraction radii $R_{\rm ex}$, chosen in a range of 40 M to 90 M from the center of the collision. We decompose Ψ_4 into multipoles ψ_{lm} using spherical harmonics of spin weight -2, ${}_{-2}Y_{lm}$, according to $rM\Psi_4(t, r, \theta, \phi) = \sum_{l=2}^{\infty} \sum_{m=-l}^{l} {}_{-2}Y_{lm}(\theta, \phi)\psi_{lm}(t, r)$. Because of the symmetry properties of the systems under consideration, the only nonvanishing multipoles all have $m = 0$ in a suitably chosen frame, and are purely real, corresponding to a single polarization state h_+. In the equal-mass limit, the additional symmetry causes all multipoles with odd l to vanish identically. The energy spectrum and luminosity of the radiation are given by

$$\frac{dE}{d\omega} = \sum_l \frac{1}{16\pi^2} \frac{|\hat{\psi}_{l0}(\omega)|^2}{\omega^2} \equiv \sum_l \frac{dE_l}{d\omega}, \quad (2)$$

$$\frac{dE}{dt} = \sum_l \frac{1}{16\pi M^2} \left| \int_{-\infty}^{t} \psi_{l0}(\tilde{t}) d\tilde{t} \right|^2 \equiv \sum \frac{dE_l}{dt}, \quad (3)$$

respectively, where a hat denotes the Fourier transform and ψ_{l0} is evaluated on a sphere at infinity.

III. SIMULATIONS AND UNCERTAINTIES

We have performed a series of simulations of head-on collisions with mass ratio ranging from $q = 1$ to $q = 1/100$ with initial coordinate separation d and proper horizon-to-horizon separation L as given in Table I. We describe the grid setup used for these simulations in terms of the number $n_{\rm rl}$ of refinement levels, the radius R of the computational domain, the resolution H used in the wave extraction zone,[1] the radius r in units of the smaller hole's mass m_2 of the innermost refinement level centered on the individual punctures[2] and the resolution h/m_2 of the innermost refinement level. The values for these parameters are summarized for all mass ratios in Table II.

[1]Typically the third refinement level counted from the outside.

[2]For the small mass ratios $q = 1/10$ $(1/100)$, the two (five) highest resolution boxes are placed around the small hole only to reduce computational cost.

TABLE I. Mass ratio q, coordinate and proper separation d and L, respectively, as well as radiated energy $E_{\rm rad}$ with percentage distribution in the $l=2$, $l=3$ and $l=4$ multipoles and recoil velocity v for the set of binary models evolved numerically.

q	d/M	L/M	$E^{\rm rad}/M$	$E^{\rm rad}_{l=2,3,4}(\%)$			$v/(\mathrm{km/s})$
1	10.24	12.48	5.32×10^{-4}	99.6	0	0.03	0
1	12.74	16.76	5.39×10^{-4}	99.3	0	0.03	0
1	17.51	21.82	5.56×10^{-4}	99.4	0	0.03	0
1/2	12.74	16.69	4.33×10^{-4}	98.1	1.28	0.07	3.71
1/3	12.74	16.60	3.11×10^{-4}	96.7	2.83	0.16	3.97
1/4	7.31	10.57	2.16×10^{-4}	95.8	3.85	0.25	3.65
1/4	12.74	16.53	2.28×10^{-4}	95.4	4.14	0.28	3.72
1/4	17.51	21.61	2.33×10^{-4}	95.6	4.13	0.27	3.83
1/10	12.72	16.28	6.05×10^{-5}	92.1	7.09	0.67	1.31
1/10	16.72	20.55	6.16×10^{-5}	92.5	7.23	0.70	1.33
1/10	20.72	24.76	6.29×10^{-5}	92.0	7.15	0.67	1.34
1/100	7.15	9.58	9.10×10^{-7}	88.1	9.01	1.15	0.0243
1/100	11.87	15.08	9.65×10^{-7}	88.0	9.87	1.46	0.0248
1/100	13.85	17.21	9.94×10^{-7}	87.8	10.11	1.46	0.0256
1/100	15.08	18.53	1.012×10^{-6}	87.7	10.05	1.51	0.0260

TABLE II. Grid setup used for the different mass ratios q. The number of refinement levels is given by $n_{\rm rl}$, R is the radius of the computational domain, H the resolution in the wave extraction zone, r the radius of the innermost refinement box around the individual punctures and h the resolution used on that level. The additional low and high resolution for $q=1/4$ and $q=1/100$ have been used for the convergence studies.

q	$n_{\rm rl}$	R/M	H/M	r/m_2	h/m_2
1	9	512	0.76	2	1/21
1/2	9	341	0.51	2	1/21
1/3	9	256	0.76	2	1/21
1/4	9	205	(1.22, 1.07, 0.95)	1	(1/21, 1/24, 1/27)
1/10	12	303	0.73	0.625	1/64
1/100	15	223	(1.01, 0.63, 0.51)	0.625	(1/40, 1/64, 1/80)

Our results are affected by three main sources of uncertainties: finite extraction radius, discretization and, for small initial separations of the binary, spurious initial radiation. We reduce the error arising from finite extraction radius by measuring the wave form components at several radii, and fitting them to an expression of the form $\psi_{lm}(r,t)=\psi^{(0)}_{lm}(t)+\psi^{(1)}_{lm}(t)/r$. The wave form "at infinity" $\psi^{(0)}_{lm}(t)$ is the quantity reported throughout this work and used to calculate related quantities, such as the radiated energy. The uncertainty in this extrapolated value is estimated by performing a second fit including also a quadratic term $\psi^{(2)}_{lm}/r^2$, and taking the difference between the first- and second-order fits. The resulting uncertainty increases as we decrease the mass ratio q and is 1–4% for the total radiated energy and the $l=2$ wave form and energy, and 3–5% for the subdominant multipoles and the radiated linear momentum.

In order to estimate the discretization error of our simulations, we have performed a convergence analysis for models ($q=1/4$, $L=16.53M$) and ($q=1/100$, $L=9.58M$) using the three resolutions listed for these mass ratios in Table II. The resulting convergence plots for the $l=2$ multipole of the wave signal is shown in Fig. 1 and demonstrates convergence between second and fourth order. With regard to the analysis below, we note, in particular, that the $q=1/100$ case exhibits second-order convergence in the plunge-merger signal around $t-R_{\rm ex}\approx 40M$ but is close to fourth-order convergence for the remainder of the wave form. Bearing in mind that the plunge-merger transition represents the most dynamic part of the evolution and that the second-order ingredients in the code are associated with the prolongation of grid functions at the refinement boundaries in time, this observation is compatible with the numerical discretization. We observe similar convergence properties for the $l=3$ multipole, but overall convergence close to fourth-order for the radiated energy and linear momentum, presumably because the accumulated errors are dominated by the

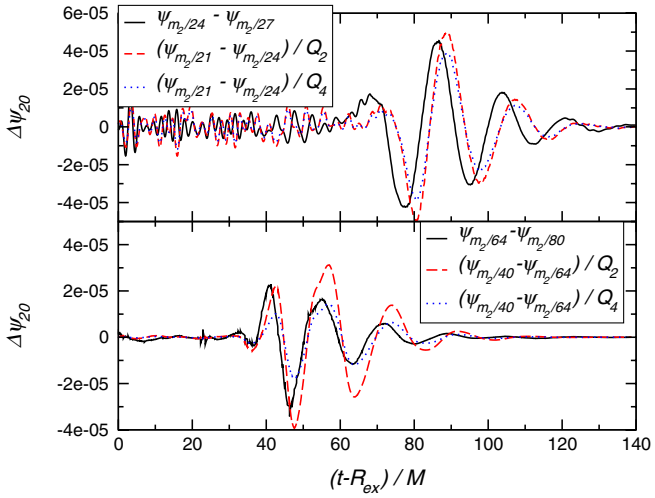

FIG. 1 (color online). Convergence analysis for the $l = 2$ multipole of the gravitational wave signal for simulation $q = 1/4$, $D = 16.53M$ (upper) and simulation $q = 1/100$, $D = 9.58$ (lower panel). In both cases we show the higher resolution differences (solid black) together with the lower resolution result rescaled for second (dashed red lines) and fourth-order convergence (dotted blue lines).

fourth-order contributions observed for most of the signal. The resulting numerical uncertainties for $q = 1/100$ are about 10% in the wave form for the plunge-merger transition and 5% for the remainder of the signal as well as 6% for the radiated energy and 8% for the linear momentum lost in gravitational waves. We note that in both cases, the discretization error leads to an overestimate of the radiated quantities. For $q = 1/4$ we observe significantly smaller uncertainties in the range of 2% for all quantities.

Finally, we comment on the unphysical gravitational radiation inherent in the conformally flat puncture initial data. In order to extract physically meaningful information, one has to separate the spurious radiation from the radiation generated by the collision itself. This is done by ''waiting'' for the spurious radiation to radiate off the computational domain, and then discarding the early, contaminated part of the wave signal. For small values of the initial separation, however, the binary will merge before the spurious radiation has had enough time to leave the system, and physical and unphysical contributions to the wave signal partially overlap and cannot be cleanly distinguished. For our set of simulations, this problem arises only in the case $q = 1/100$, $L = 9.58M$, where it introduces an additional error of about 2% to the radiated energy and momentum.

IV. RESULTS

All collisions summarized in Table I result in the formation of a single BH plus gravitational radiation, i. e. there is no indication of violation of the cosmic censorship conjecture. The final BH is born distorted, and eventually rings down to a Schwarzschild solution via emission of a superposition of quasinormal modes [50].

We illustrate the $l = 2$ and $l = 3$ wave signal in Fig. 2 for the $l = 2$ and $l = 3$ multipoles obtained for the mass ratios $q = 1/4$ (top), $q = 1/10$ (center) and $q = 1/100$ (bottom). In each panel the solid (black) curves represent the PP prediction for infall from infinity whereas the dotted (red) and dash-dotted (blue) curves show the numerical results for different values of the finite initial separation. To leading order, the gravitational radiation output of black-hole collisions scales with the square of the reduced mass $\mu \equiv M\eta$ of the system, where $\eta = q/(q+1)^2$ is the dimensionless, symmetric mass ratio [24]. For comparison of the numerical results with PP predictions, we therefore rescale the former by the corresponding powers of η, quadratic for energy and linear for the wave forms in Fig. 2.

The wave forms show interesting features. For small initial separations, the early part of the wave form is contaminated by ''spurious'' radiation; cf. the dotted (red) curve in the top and bottom panels of Fig. 2. As the initial separation increases, however, this problem disappears, because the longer infall duration of the binary provides sufficient time for the unphysical radiation to propagate off the grid; cf. the dash-dotted (blue) curves. A closer inspection of the $q = 1/100$ case yields excellent agreement between the numerical and PP predictions except for the plunge-merger transition around $t \approx 0$ in the figure. From the discussion in Sec. III, however, we recall that the discretization error is particularly large in this regime. In fact, for the $q = 1/100$ model studied in Sec. III, a second-order Richardson extrapolation predicts about a 10% reduction in the amplitude around the first strong maximum in the $l = 2$ wave form which is very close in magnitude and sign to the deviation of the numerical from the PP result. As demonstrated by the upper central panel in Fig. 2, we find equally good agreement of the numerical $l = 2$ multipole with PP predictions for the less extreme mass ratio $q = 1/10$ and only a small deviation for the larger mass ratio $q = 1/4$ (upper top panel in Fig. 2). Our findings thus confirm over a wide range of mass ratios the observation by Ref. [35], that there is a weak dependence of the rescaled wave forms on the mass ratio. The $l = 3$ mode, on the other hand, is a good discriminator between high- and low-mass ratios. This behavior was qualitatively expected, as higher multipoles are suppressed in the equal-mass case; by symmetry the $l = 3$ mode is absent when the masses are equal. It is interesting, however, that even for what one might call a small mass ratio, $q = 1/10$, higher multipoles are still visibly suppressed.

The total amount of energy radiated in gravitational waves during the collision depends on the initial separation of the holes. As discussed in Anninos *et al.* [35], two effects contribute to increasing the GW energy at larger

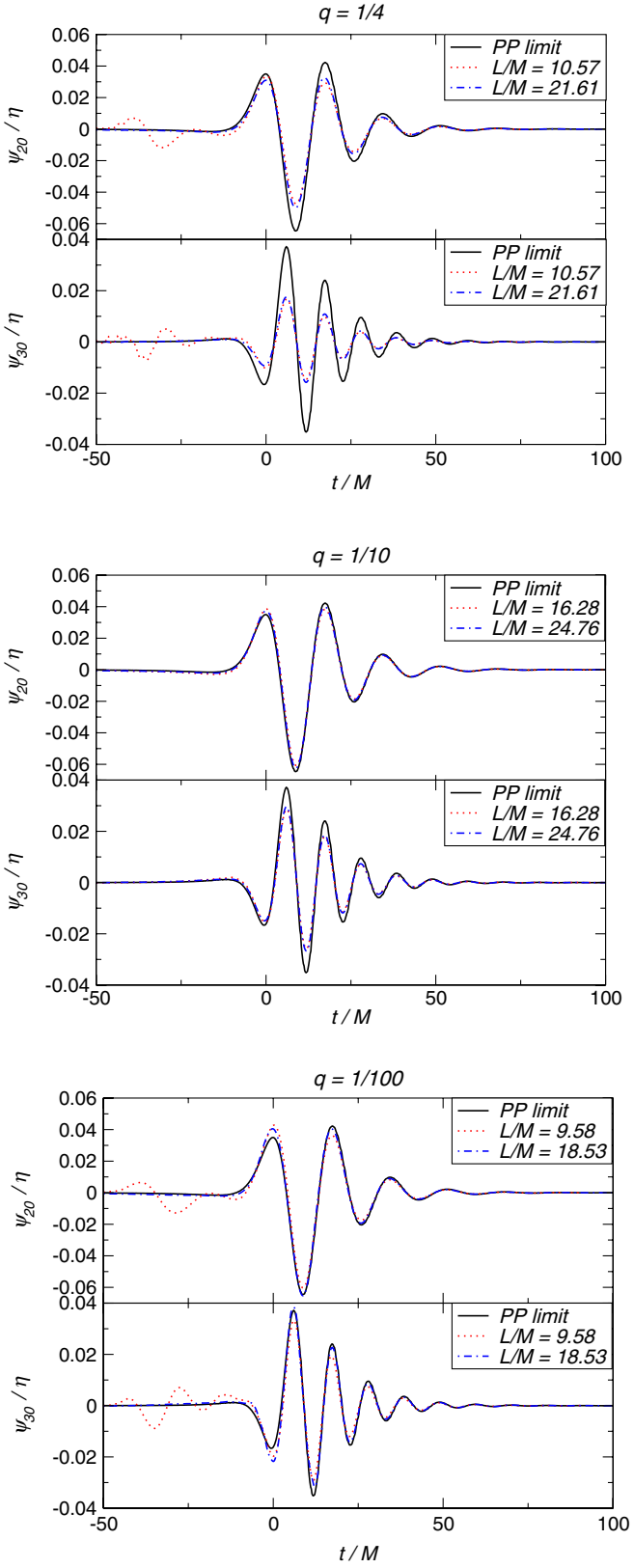

FIG. 2 (color online). Rescaled wave forms for mass ratios $q = 1/4$ (top), $q = 1/10$ (center) and $q = 1/100$ (bottom panels) for $l = 2$ (upper) and $l = 3$ (lower half of each panel), for two different initial separations. Also shown is the wave form in the PP limit (black solid lines).

initial separations; (i) there is more time to radiate GWs during the infall and (ii) the infalling velocity is larger. In practice, the second effect is found to be dominant. Anninos *et al.* have accounted for both contributions by defining

$$F_L = \frac{\int_L^{2M} \dot{r}\dot{r}^2 dr}{\int_\infty^{2M} \lim_{L\to\infty} \dot{r}\,\dot{r}^2 dr},$$

$$\dot{r} = \frac{(1-2M/r)\sqrt{2ML/r - 2M}}{\sqrt{L-2M}}.$$

One can write the corrections to the radiation emission

$$E_L^{\rm rad} = F_L E_\infty^{\rm rad} = \left(1 - \frac{40M}{9L}\right) E_\infty^{\rm rad} + \mathcal{O}\left(\frac{M^2}{L^2}\right).$$

With the above as motivation, we have fitted our results to a $1/L$ dependence, of the form

$$\frac{E^{\rm rad}(L)}{M\eta^2} = \frac{E_\infty^{\rm rad}}{M\eta^2}(1 + a_E M/L), \tag{4}$$

with $E_\infty^{\rm rad}$ the radiated energy for infinite initial separation. The results are summarized in Table III. We remind the reader that L stands for proper initial separation between the holes. We also note that the results in Table III are normalized by η^2. For comparison, we also show in the last entry of the table the results obtained in the PP limit, within a linearized calculation. This study was done by Lousto and Price [30] using the same type of initial data; we have used their Table I to obtain the behavior shown in Table III above. We note that already for $q = 1/10$ and $q = 1/100$ our results are in good agreement with PP calculations. We remind the reader, however, that in the $q = 1/10$ case there is a larger deviation in the $l = 3$ modes.

With the extrapolation above one gets an estimate for the total radiation of two black holes merging from infinite initial separation. A best fit of this number as function of mass ratio yields

$$\frac{E_\infty^{\rm rad}}{M\eta^2} = 0.0110 - 0.0088\eta \tag{5}$$

In the PP limit, when $\eta \to 0$, this agrees with the classical PP calculation, Eq. (1) to within 6%, so within the numerical uncertainties. Overall, the results in Table I demonstrate that we are able to accurately measure amounts of order $E^{\rm rad} \sim 10^{-6}M$ in these fully nonlinear evolutions.

TABLE III. Summary of our results when fitted to Eqs. (4) and (6). The last column refers to PP results, as extrapolated from Lousto and Price [30].

q	1/1	1/4	1/10	1/100	PP
$E_\infty^{\rm rad}/(M\eta^2)$	0.009 36	0.009 11	0.009 85	0.0114	0.0104
v_∞^f(km/s)	0.0	258.0	250.3	275.9	257.6

The amount of spurious radiation in the initial data is also consistent with predictions from linearized gravity. Lousto and Price performed a detailed analysis of the amount of spurious radiation in the infall of PPs into massive black holes, using the same type of initial data [30]. Using their Table I for $L > 11$, we find that the amount of spurious radiation varies with L according to $E_{\rm rad}/(M\eta^2) \sim 0.15(L/M)^{-2.5}$. For $q = 1/100$, for instance, we obtain $E_{\rm rad}/(M\eta^2) = 0.26(L/M)^{-2.55}$. Thus, we find good agreement in the decay power (roughly -2.5) and also in the proportionality coefficient.

If two BHs with different masses collide head-on, the remnant BH will recoil with respect to the center-of-mass frame, due to the emission of energy and momentum carried by gravitational waves. Based on PN tools, we have fit our results to [51]

$$v_{\rm recoil} = v^f_\infty \frac{q^2(1-q)}{(1+q)^5}(1 + b_E M/L), \tag{6}$$

where v^f_∞ is a normalized recoil velocity for infinite initial separation. The normalized recoil velocity v^f_∞ is shown in Table III. The point particle limit was considered in Ref. [52], who obtained $v^f_\infty = 263$ km/s.[3] We note this is not a trivial agreement: unlike energy calculations, momentum involves interference with higher (typically highly suppressed) multipoles. Overall, our results agree well in the limit of small mass-ratios with the point particle limit. It is interesting to note in this context that for both, radiated energy and linear momentum, the numerical results exceed those obtained from the point particle limit by about 6%. This value agrees in sign and magnitude with the discretization error obtained for the $q = 1/100$ simulation in Sec. III. We therefore consider the discretization error the dominant source of the remaining discrepancies.

V. CONCLUSIONS

The simulation of dynamical, interacting black holes has a tremendous potential to provide answers to some of the most fundamental questions in physics. Recent developments in experimental and theoretical physics make this a pressing issue. We refer, in particular, to the prominent role of BHs in the gauge-gravity duality, in TeV-scale gravity or even on their own as solutions of the field equations [53]. Recent work along these lines includes the successful simulation and understanding of the collision of two BHs at close to the speed of light in four-dimensional spacetime [54–57], the low energy collisions in higher spacetime dimensions [53,58,59], BH scattering in five dimensions [60], stability studies in higher dimensions [61–63] and BH evolutions in non asymptotically flat spacetimes [64] (for the formalism extension, we refer the reader to Refs. [53,58,65–68]).

We have shown here that numerical relativity is capable of simulating dynamical black holes close to the regime of validity of linear calculations, and to make contact with (semi-)analytic approximation techniques. For this purpose we have evolved head-on collisions of nonspinning black-hole binaries over a range of mass ratios from $q = 1$ to $q = 1/100$. We obtain radiated energies decreasing from about 5.5×10^{-4} for $q = 1$ to 10^{-6} for $q = 1/100$. The recoil reaches a maximum of about 4 km/s near $q = 3$ and decreases towards 26 m/s for $q = 1/100$. In the limit of small mass ratios and extrapolating our results to infinite initial separation, we find the numerical values for radiated energy and linear momentum to be $\approx 6\%$ larger than the point-particle predictions. This discrepancy agrees rather well in sign and magnitude with the discretization error obtained from a convergence study of our $q = 1/100$ simulations. It thus appears likely that a significant part of the remaining differences can be attributed to the discretization error which mirrors the computational demands of numerical black-hole binary simulations with such small mass ratios.

With regard to the wave forms, the most remarkable result is the suppression of odd l multipoles. While we observe good agreement between numerical and point-particle results for the $l = 2$ mode, already for $q = 1/10$, the numerically calculated $l = 3$ multipole is visibly suppressed for this case and only agrees well with the PP limit for $q = 1/100$.

Overall, the good agreement for wave forms and radiated energy and momenta for the case $q = 1/100$ demonstrates that numerical techniques are capable of bridging the gap between linear analysis and the fully nonlinear regime of general relativity.

ACKNOWLEDGMENTS

We thank E. Mitsou for sharing data from his earlier work [33], which helped assess the accuracy of our own PP wave forms and fluxes. U. S. acknowledges support from the Ramón y Cajal Programme of the Ministry of Education and Science of Spain, FP-7-PEOPLE-2011-CIG Grant CBHEO, No. 293412, NSF Grant Nos. PHY-0601459, PHY-0652995 and the Sherman Fairchild Foundation to Caltech. H. W. is funded by FCT through Grant No. SFRH/BD/46061/2008. This work was supported by the DyBHo-256667 ERC Starting Grant and by FCT—Portugal through Project Nos. PTDC/FIS/098025/2008, PTDC/FIS/098032/2008 CTE-AST/098034/2008 and CERN/FP/116341/2010, by the NSF under Grant Nos. PHY-090003, PHY-100033, and OCI-0905046, Grant Nos. ICTS-CESGA-175 and ICTS-CESGA-200, AECT-2011-02-0006 and AECT-2011-02-0015. C. D. O. acknowledges support from the NSF under Grant No. AST-0855535. E. S. acknowledges support from the

[3]Note the slight disagreement with the extrapolation of Lousto and Price's results, shown in Table III

NSF under Grant No. 0721915 (Alpaca) and NSF Grant No. 0904015 (CIGR). We acknowledge the support of the National Institute for Computational Sciences (NICS) of the University of Tennessee, the San Diego Supercomputing Center (SDSC), the Centro de Supercomputación de Galicia (CESGA) and the Barcelona Supersomputing Center (BSC). Computations were performed on the TeraGrid clusters NICS Kraken, SDSC Trestles, on CESGA's Finis Terrae cluster, on the University of Zaragoza's BIFI Caesaraugusta, on the Milipeia cluster in Coimbra, BSC's Mare Nostrum and LRZ Munich.

[1] F. Pretorius, Phys. Rev. Lett. **95**, 121101 (2005).
[2] M. Campanelli, C. O. Lousto, P. Marronetti, and Y. Zlochower, Phys. Rev. Lett. **96**, 111101 (2006).
[3] J. G. Baker, J. Centrella, D.-I. Choi, M. Koppitz, and J. van Meter, Phys. Rev. Lett. **96**, 111102 (2006).
[4] E. Berti *et al.*, Phys. Rev. D **76**, 064034 (2007).
[5] J. Centrella, J. G. Baker, B. J. Kelly, and J. R. van Meter, Rev. Mod. Phys. **82**, 3069(2010).
[6] U. Sperhake, E. Berti, and V. Cardoso, arXiv:1107.2819.
[7] T. Damour, A. Nagar, and M. Trias, Phys. Rev. D **83**, 024006 (2011).
[8] Y. Pan *et al.*, Phys. Rev. D **81**, 084041 (2010).
[9] L. Santamaria *et al.*, Phys. Rev. D **82**, 064016 (2010).
[10] J. Abadie *et al.* (The LIGO Scientific Collaboration and the Virgo Collaboration), Phys. Rev. D **83**, 122005 (2011).
[11] I. MacDonald, S. Nissanke, H. P. Pfeiffer, and H. P. Pfeiffer, Classical Quantum Gravity **28**, 134002 (2011).
[12] J. A. Gonzalez, M. Hannam, U. Sperhake, B. Brügmann, and S. Husa, Phys. Rev. Lett. **98**, 231101 (2007).
[13] M. Campanelli, C. O. Lousto, Y. Zlochower, and D. Merritt, Phys. Rev. Lett. **98**, 231102 (2007).
[14] M. Campanelli, C. O. Lousto, Y. Zlochower, and D. Merritt, Astrophys. J. **659**, L5 (2007).
[15] M. Kesden, U. Sperhake, and E. Berti, Phys. Rev. D **81**, 084054 (2010).
[16] M. Kesden, U. Sperhake, and E. Berti, Astrophys. J. **715**, 1006 (2010).
[17] E. Berti *et al.*, Phys. Rev. D **81**, 104048 (2010).
[18] T. Hinderer and E. E. Flanagan, Phys. Rev. D **78**, 064028 (2008).
[19] L. Barack, Classical Quantum Gravity **26**, 213001 (2009).
[20] P. Canizares and C. F. Sopuerta, Phys. Rev. D **79**, 084020 (2009).
[21] N. Yunes *et al.*, Phys. Rev. D **83**, 044044 (2011).
[22] P. A. Sundararajan, G. Khanna, and S. A. Hughes, Phys. Rev. D **81**, 104009 (2010).
[23] E. Poisson, A. Pound, and I. Vega, arXiv:1102.0529.
[24] M. Davis, R. Ruffini, W. Press, and R. Price, Phys. Rev. Lett. **27**, 1466 (1971).
[25] J. A. Gonzalez, U. Sperhake, and B. Brügmann, Phys. Rev. D **79**, 124006 (2009).
[26] C. O. Lousto, H. Nakano, Y. Zlochower, and M. Campanelli, Phys. Rev. Lett. **104**, 211101 (2010).
[27] C. O. Lousto, H. Nakano, Y. Zlochower, and M. Campanelli, Phys. Rev. D **82**, 104057 (2010).
[28] C. O. Lousto and Y. Zlochower, Phys. Rev. Lett. **106**, 041101 (2011).
[29] H. Nakano, Y. Zlochower, C. O. Lousto, and M. Campanelli, arXiv:1108.4421.
[30] C. O. Lousto and R. H. Price, Phys. Rev. D **69**, 087503 (2004).
[31] C. O. Lousto and R. H. Price, Phys. Rev. D **55**, 2124 (1997).
[32] V. Cardoso and J. P. Lemos, Phys. Lett. B **538**, 1 (2002).
[33] E. Mitsou, Phys. Rev. D **83**, 044039 (2011).
[34] Z. Andrade and R. H. Price, Phys. Rev. D **56**, 6336 (1997).
[35] P. Anninos, D. Hobill, E. Seidel, L. Smarr, and W.-M. Suen, Phys. Rev. D **52**, 2044 (1995).
[36] P. Anninos and S. Brandt, Phys. Rev. Lett. **81**, 508 (1998).
[37] C. Reisswig, C. D. Ott, U. Sperhake, and E. Schnetter, Phys. Rev. D **83**, 064008 (2011).
[38] U. Sperhake, Phys. Rev. D **76**, 104015 (2007).
[39] U. Sperhake *et al.*, Phys. Rev. D **78**, 064069 (2008).
[40] T. Goodale *et al.*, in *Vector and Parallel Processing–VECPAR'2002*, 5th International Conference, Lecture Notes in Computer Science (Springer, Berlin, 2003).
[41] Cactus Computational Toolkit, http://www.cactuscode.org/.
[42] E. Schnetter, S. H. Hawley, and I. Hawke, Classical Quantum Gravity **21**, 1465 (2004).
[43] Mesh refinement with Carpet, http://www.carpetcode.org/.
[44] J. Thornburg, Phys. Rev. D **54**, 4899 (1996).
[45] J. Thornburg, Classical Quantum Gravity **21**, 743 (2004).
[46] M. Ansorg, B. Brügmann, and W. Tichy, Phys. Rev. D **70**, 064011 (2004).
[47] M. Shibata and T. Nakamura, Phys. Rev. D **52**, 5428 (1995).
[48] T. W. Baumgarte and S. L. Shapiro, Phys. Rev. D **59**, 024007 (1998).
[49] M. Alcubierre *et al.*, Phys. Rev. D **67**, 084023 (2003).
[50] E. Berti, V. Cardoso, and A. O. Starinets, Classical Quantum Gravity **26**, 163001 (2009).
[51] M. J. Fitchett, Mon. Not. R. Astron. Soc. **203**, 1049 (1983).
[52] T. Nakamura and M. Haugan, Astrophys. J. **269**, 292 (1983).
[53] M. Zilhao *et al.*, Phys. Rev. D **81**, 084052 (2010).
[54] U. Sperhake, V. Cardoso, F. Pretorius, E. Berti, and J. A. Gonzalez, Phys. Rev. Lett. **101**, 161101 (2008).
[55] U. Sperhake *et al.*, Phys. Rev. Lett. **103**, 131102 (2009).
[56] U. Sperhake, E. Berti, V. Cardoso, F. Pretorius, and N. Yunes, Phys. Rev. D **83**, 024037 (2011).
[57] M. Shibata, H. Okawa, and T. Yamamoto, Phys. Rev. D **78**, 101501 (2008).
[58] H. Witek *et al.*, Phys. Rev. D **82**, 104014 (2010).

[59] H. Witek *et al.*, Phys. Rev. D **83**, 044017 (2011).
[60] M. Shibata, Y. Suwa, K. Kiuchi, and K. Ioka, Phys. Rev. D **83**, 121501 (2011).
[61] M. Shibata and H. Yoshino, Phys. Rev. D **81**, 021501 (2010).
[62] M. Shibata and H. Yoshino, Phys. Rev. D **81**, 104035 (2010).
[63] L. Lehner and F. Pretorius, Phys. Rev. Lett. **105**, 101102 (2010).
[64] H. Witek *et al.*, Phys. Rev. D **82**, 104037 (2010).
[65] H. Yoshino and M. Shibata, Phys. Rev. D **80**, 084025 (2009).
[66] E. Sorkin and M. W. Choptuik, Gen. Relativ. Gravit. **42**, 1239 (2009).
[67] E. Sorkin, Phys. Rev. D **81**, 084062 (2010).
[68] K. A. Dennison, J. P. Wendell, T. W. Baumgarte, and J. D. Brown, Phys. Rev. D **82**, 124057 (2010).